Digest Journal of Nanomaterials and Biostructures Vol. 6, No 3, July - September 2011, p. 1393-1401

# SYNTHESIS AND CHARACTERIZATION OF ZnO NANOPOWDER BY NON-BASIC ROUTE

O. OPREA*, E. ANDRONESCU, B. S. VASILE, G. VOICU, C. COVALIU
*University Politehnica of Bucharest, Faculty of Applied Chemistry and Materials Science, Romania*

Nanocrystalline ZnO particles were prepared from methanolic solutions of zinc acetate dihydrate without using base such as NaOH or LiOH through a colloid process carried out at a low temperature of 60°C. The precipitate obtained after 12-72h contained ZnO, covered with polymeric species of zinc hydroxo acetate. The reaction course was studied by mass spectrometry means. To complete the hydrolysis process, up to pure ZnO, it was necessarily to reflux the white precipitate separate from methanolic solution, in water at 80°C. We found that reaction time in the presence of methanol primarily influenced the size of the particles, while the reaction time in the presence of water mainly influenced the ZnO purity.

(Received August 24, 2011; accepted September 23, 2011)

*Keywords*: Zinc oxide, nanosize, zinc acetate, non-basic hydrolysis

## 1. Introduction

Semiconductor nanoparticles have attracted interests of many academic and industrial researchers because of their unusual optoelectronic properties. Wurtzite ZnO is an n-type semiconductor with a wide band-gap. Nanosized ZnO can be utilized in electrochemical fields including chemical sensors [1], photocatalysts [2, 3], phosphors [4], thin films [5] and dye-sensitized solar cells [6], but is also used in a series of cosmetic preparates, sun protection cream, acne treatment, wound dressing or other bacteriostatic products [7]. Application of zinc oxide has been shown to accelerate the healing of both chronic and acute wounds and it also exhibit antibacterial and anti-inflammatory behaviour.

ZnO have also been prepared by novel methods, using various templates and surfactants, as starch [8], CTAB [9], but in general, nanocolloids or nanopowders of ZnO have been prepared by adapting synthetic methods developed by Koch et al. [10], Bahnemann et al. [11], or Spanhel et al. [12]. Zinc salts are dissolved in alcoholic or other organic solvents to which basic solutions containing NaOH, LiOH or $NH_4OH$ are added. It is believed that formation of colloidal ZnO follows several reaction steps, of which the last is transformation of zinc hydroxide to zinc oxide under basic solution conditions. In the presence of the acetate ions in the basic solutions, the precursors of ZnO are reported to be $Zn_{10}O_4(Ac)_{12}$, $Zn_4O(Ac)_6$, or $Zn_5(OH)_8(Ac)_2 \cdot 2H_2O$ [13]. Hydrolysis and condensation of these precursors lead to the precipitation of ZnO in the presence of base.

It has been reported [13] that nanocrystalline ZnO particles can be successfully prepared through controlled hydrolysis of zinc acetate, but were heavily impurified by layered hydroxide zinc acetate, $Zn_5(OH)_8(Ac)_2 \cdot 2H_2O$

In view of fundamental studies as well as industrial applications of nanoparticles, chemically pure or compositionally well-defined ZnO is required. Therefore developing a method of obtaining cheap, pure ZnO with small, controlled size is highly desirable.

*Corresponding author: ovidiu73@yahoo.com

In this study, nanocrystalline ZnO particles were successfully prepared through controlled hydrolysis of zinc acetate under moderate conditions such as neutral solutions, low temperature, and ambient atmosphere, without using any alkaline solution.

## 2. Experimental procedure

Zinc acetate dihydrate, $Zn(Ac)_2 \cdot 2H_2O$, with 99.9% purity was obtained from Merck. Absolute methanol (MeOH) was used as received from Sigma without further purification.

ZnO synthesis

2.1940g (0.01 moles) $Zn(CH_3COO)_2\ 2H_2O$ were dissolved in 50 mL methanol. The solution was then kept for 12-72h on a thermostatic bath at 60°C. The white colloidal precipitate formed was then separated by centrifugation at 18.000 rpm and washed several times with methanol. The white powder was suspended in 50 mL bi-distilled water and kept for 12-72h on a thermostatic bath at 80°C. The white colloidal precipitate was then again separated by centrifugation at 18.000 rpm for 10 min. Final product was dried at 105°C for 30 min in the ambient atmosphere following the removal of supernatant.

**Experimental techniques**

a) Electron Microscope Images. The micrographs were obtained using a Tecnai™ $G^2$ F30 S-TWIN transmission electron microscope from FEI the Nederland's, equipped with STEM/HAADF detector, EDX (Energy dispersive X-ray Analysis) and EFTEM - EELS (Electron energy loss spectroscopy) operated at an acceleration voltage of 300 KV obtained from a Shottky Field emitter with a TEM point resolution of 2 Å and line resolution of 1.02 Å.

b) X-ray Diffraction. X-ray powder diffraction patterns were obtained with a Shimadzu XRD6000 diffractometer, using Cu Kα (1.5406 Å) radiation operating with 30 mA and 40 kV in the 2θ range 10–70°. A scan rate of $1^o\ min^{-1}$ was employed.

c) Infrared Spectroscopy. The Fourier transform infrared (FTIR) spectra were recorded using the KBr pellet technique on a Bruker Tensor 27 spectrometer in the 4000–400 $cm^{-1}$ frequency range. A total of 30 scans and a resolution of 1 $cm^{-1}$ were employed in getting the spectra.

d) Chemical analysis. Elemental microanalyses (carbon and hydrogen) were carried out using a Perkin-Elmer Model 2400 CHN Analyzer.

e) Thermal analysis. Thermal behaviour of the ZnO nanopowder was followed by TG-DSC with a Netzsch TG 449C STA Jupiter. Sample was placed in alumina crucible and heated with $10K \cdot min^{-1}$ from room temperature to 650° C, under the flow of 10 mL $min^{-1}$ dried air.

f) Photoluminescence spectra. Photoluminescence spectra (PL) were measured with a Perkin Elmer P55 spectrometer using a Xe lamp as a UV light source at ambient temperature, in the range 200-800 nm, with all the samples in solid state. The measurements were made with scan speed of 200 $nm \cdot min^{-1}$, slit of 10 nm, and cut-off filter of 1%. An excitation wavelength of 320 nm was used.

g) MS study was carried out with a LC-MS (ESI-MS) MSQ Plus Thermo Fisher Scientific apparatus, with monoquadrupol, in positive electrospray ionization. The probes were dissolved in acetonitrile and were introduced in the MS with a debt of 0.5 mL/min by a quaternary HPLC pump. The working conditions (T=450°C and con voltage Vc=40V) were chosen to obtain a minimum fragmentation of the injected species.

h) Diffuse reflectance spectra measurements were made with a JASCO V560 spectrophotometer with solid sample accessory, in the domain 200-800nm, with a speed of $200nm \cdot min^{-1}$.

i) X–ray photoelectron spectroscopy (XPS) were monitored using a Sigma Probe ThermoVG spectrometer with an excitation source of Al Kα = 1486.6 eV.

## 3. Results and discussions

In order to obtain a single-phase compound, the purification steps were monitored by FTIR spectroscopy. figure 1 shows the FT-IR spectra for the ZnO powders obtained at different

refluxing times from methanol or methanol and water. For the powders obtained only from methanol, absorption bands near 3400 $cm^{-1}$ represent O-H mode, those at 2900 $cm^{-1}$ are C-H mode, and 1400-1600 $cm^{-1}$ are the C=O asymmetric stretching mode. As the powders are also refluxed in water, the organic band at 1400-1600 $cm^{-1}$ is removed and bonding between Zn-O (473 $cm^{-1}$, 532 $cm^{-1}$) is clearly represented. It can be deduced that the ZnO formation process is essentially complete after 24h refluxing in water.

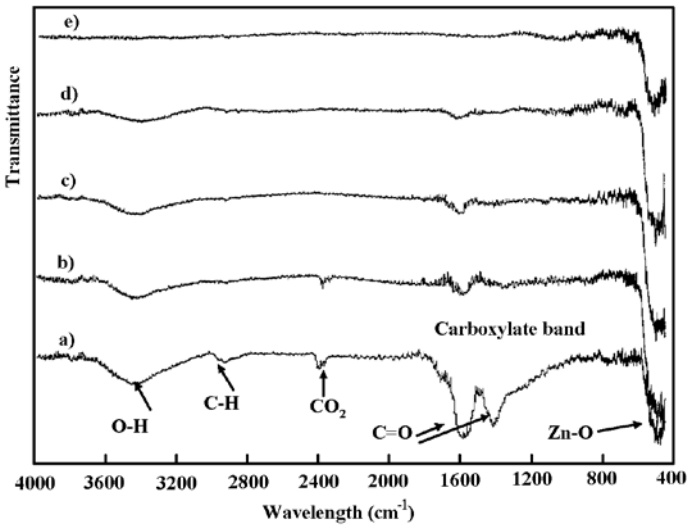


*Fig. 1. The FT-IR spectra of ZnO nanopowder obtained from different refluxing times: a) 24h in methanol; b) 24h in methanol and 6h in water; c) 24h in methanol and 12h in water; d) 24h in methanol and 18h in water; e) 24h in methanol and 24h in water.*

The thermal analysis demonstrated also the increasing purity of ZnO with increasing of reflux time in water and confirms the FTIR data, that after 24h refluxing in water the ZnO formation process is completed. For the probes a) and b) (figure 2) there are two steps of decomposition corresponding to $Zn_5(OH)_8(Ac)_2 \cdot 2H_2O$ dehydration process up to 140°C and zinc acetate decomposition between 240 and 280°C [13]. For the a) probe (figure 2) the mass loss is 2.92% and 4.90% respectively, this corresponding to about 25% $Zn_5(OH)_8(Ac)_2$. For the b) probe (figure 2) the mass loss is 1.21% and 2.27% respectively, this corresponding to about 10% $Zn_5(OH)_8(Ac)_2$. These values are in good agreement with the elemental analysis for C and H. The c) probe presents no decomposition step indicating the complete formation of ZnO.

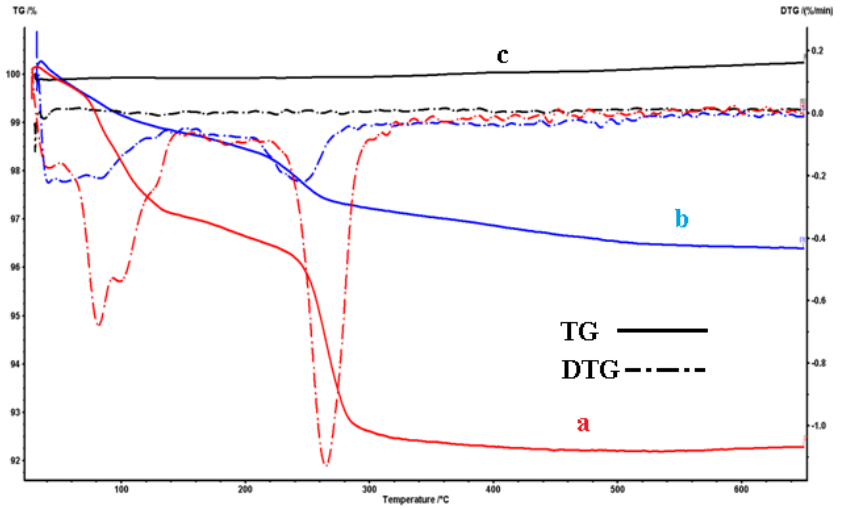


*Fig. 2. TG-DTG curves for powder obtained for refluxing: a) 24h in methanol; b) 24h in methanol and 12h in water; c) 24h in methanol and 24h in water.*

The crystalline phase formation was investigated by X-ray diffraction. The XRD data presented in figure 3a sustain also the FTIR data, demonstrating the formation of ZnO as final product. All patterns can be indexed to a hexagonal wurtzite structure.

The crystallite size of the samples can be estimated from the Scherrer equation, $D = 0.89 \cdot \lambda / \beta \cdot \cos\Theta$, where D is the average grain size, $\lambda$ is the X-ray wavelength (0.15405 nm), $\Theta$ and $\beta$ are the diffraction angle and FWHM of an observed peak, respectively. The strongest peak (101) at $2\Theta = 36.21^{o}$ was used to calculate the average crystallite size (D) of ZnO particles. The estimated average crystallite size increases from 10nm to about 40nm when increasing the refluxing time in methanol from 12 to 72h.

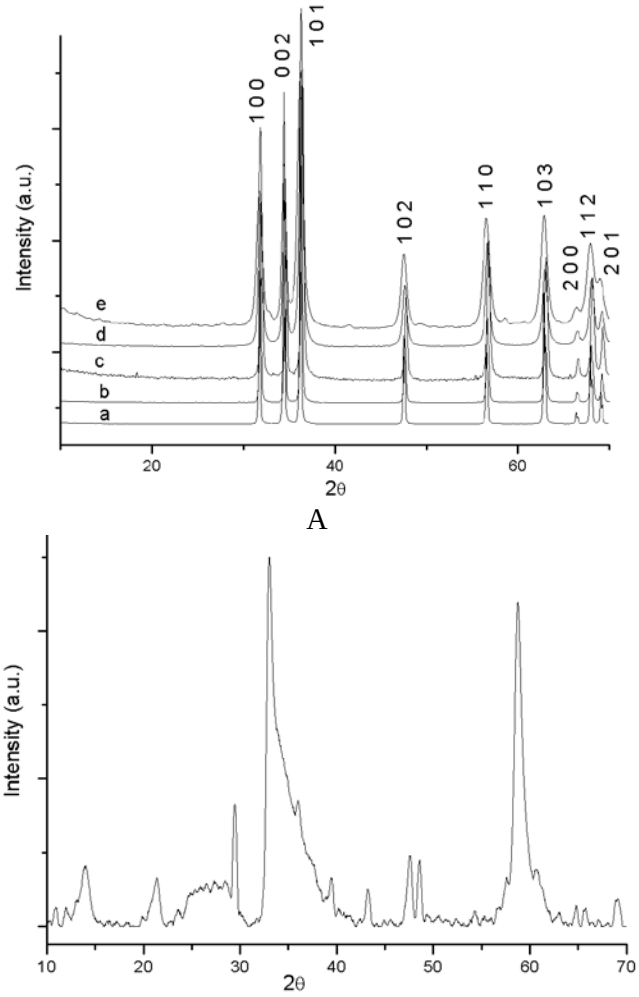


*Fig. 3. (A) XRD patterns of ZnO nanocrystals obtained for different refluxing times in methanol (a-72h, b-48h, c-36h, d-24h, and e-12h) and 24h in water; (B) The XRD pattern for the powder obtained after 24h refluxing in methanol, without water refluxing.*

It is also found that the relative intensity of (101) peak increases with increasing reflux time. This indicates a preferential orientation along the [101] direction. It should be mentioned that the most possible growth direction in ZnO is the [001] direction due to the lowest surface energy [14]. The (101) plane does not have the lowest surface energy [15]. The possible reason for the preferential orientation along the [101] direction might be explained by the formation of many {101} side planes for polyhedral-shaped particles.

The TEM bright field image, figure 4a, of ZnO nanoparticles obtained by refluxing 24h in methanol and 24h in water reveals that the powder is composed from polyhedral shaped particles, with an average particle size of approximately 18 nm. The nanopowder presents a low tendency to form soft agglomerates.

Additional information about the structures of the nanoparticles was found through detailed analysis with HRTEM. The HRTEM image, figure 4b, shows clear lattice fringes of interplanar distances of d = 2.60 Å for nanocrystalline ZnO, corresponding to Miller indices of (0 0 2) crystallographic planes of hexagonal ZnO. In addition, the regular succession of the atomic planes indicates that the nanocrystalites are structurally uniform and crystalline with almost no amorphous phase present.

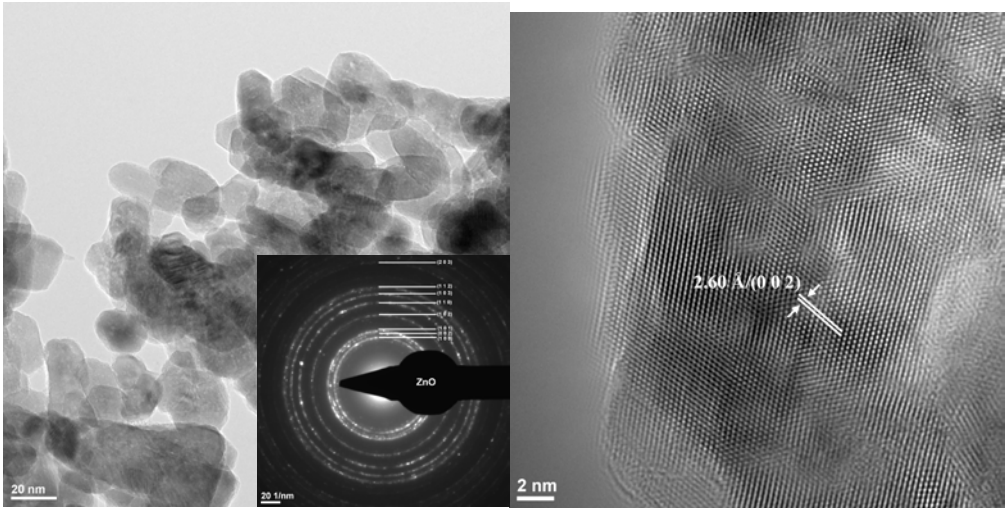


*Fig. 4. (a) TEM images of ZnO polyhedral shaped particles obtained by refluxing 24h in methanol and 24h in water; inset - SAED pattern of planes of hexagonal structure ZnO [ASTM 80-0075]; (b) HRTEM with the (0 0 2) crystallographic planes of ZnO*

From the selected area diffraction pattern obtained on ZnO nanopowder, we can state that the only phase identified is the crystalline hexagonal form of ZnO [ASTM 80-0075]. Moreover, the SAED image of ZnO nanoparticles confirms the Miller indices of characteristic crystalline structures identified by XRD (inset of figure 4a).

The XPS spectra can provide further significant information about the quality and surface composition of the ZnO nanoparticles [16]. A broad scan survey spectrum was obtained to identify the elements in the sample (ZnO nanoparticles obtained by refluxing 24h in methanol and 24h in water), figure 5.

The photoelectron peaks of the main elements, Zn, O and C, and Auger Zn LMM and O KLL peaks were obtained. Binding were corrected for specimen charging, through referencing the C 1s to 285.0 eV. The binding energy of Zn $2p_{3/2}$ was identified at 1021.0 eV.

Additionally, more information can be obtained by combining the Auger line chemical shift and the photoelectron chemical shift, the Auger parameter (α), which is a good index of the chemical state. According to Wagner et al. [17], α is given by:

$$\alpha = E_K(\text{ jkl}) + E_B(\text{i})$$

where $E_K$( jkl) is the kinetic energy of the Auger transition *jkl* and $E_B$(i) is the bonding energy of an electron in atomic level I [18]. Based on the experimental results, the α value of ZnO nanoparticles was determined to be approximately 2011 eV and can be used to compare each other's results of different XPS studies reliably because it is independent of the calibration accuracy of the binding energy scale [19-21].

An analysis of the O 1s peak (figure 5c) of ZnO reveals the fact that the peak has a slightly asymmetric line shape, with a maximum value of 530.0 eV.

This asymmetric O 1s peak was coherently fitted by three Gaussian components, centred at 529.6 eV (Oa), 530.9 eV (Ob) and 531.95 eV (Oc), respectively, as shown in figure 5c. The three fitted binding energy peaks approximate the results of Chen et al. and Wang et al. [22, 23]. Chen et al. attributed the dominant Oa peak on the low binding energy side of the O 1s spectrum to

the Zn-O bonds, related to $O^{2-}$ ions in the wurtzite structure of the hexagonal ZnO array, which are surrounded by zinc atoms with the full supplement of nearest-neighbour $O^{2-}$ ions [22]. Therefore, the Oa peak of the O 1s spectrum can be attributed to the Zn–O bonds. The intensity of the Oa peak exceeds those of the Ob and Oc peaks, indicating the strong Zn–O bonding in ZnO nanoparticles. The higher binding energy (Oc) at 531.95 eV is usually attributed to chemisorbed or dissociated oxygen or OH species on the surface of the ZnO nanoparticles, such as $CO_3^{2-}$, adsorbed $H_2O$ or adsorbed $O_2$ [22, 24, 25]. The component at the medium binding energy (Ob) of the O 1s peak is associated with $O^{2-}$ ions that are in oxygen-deficient regions within the ZnO matrix.

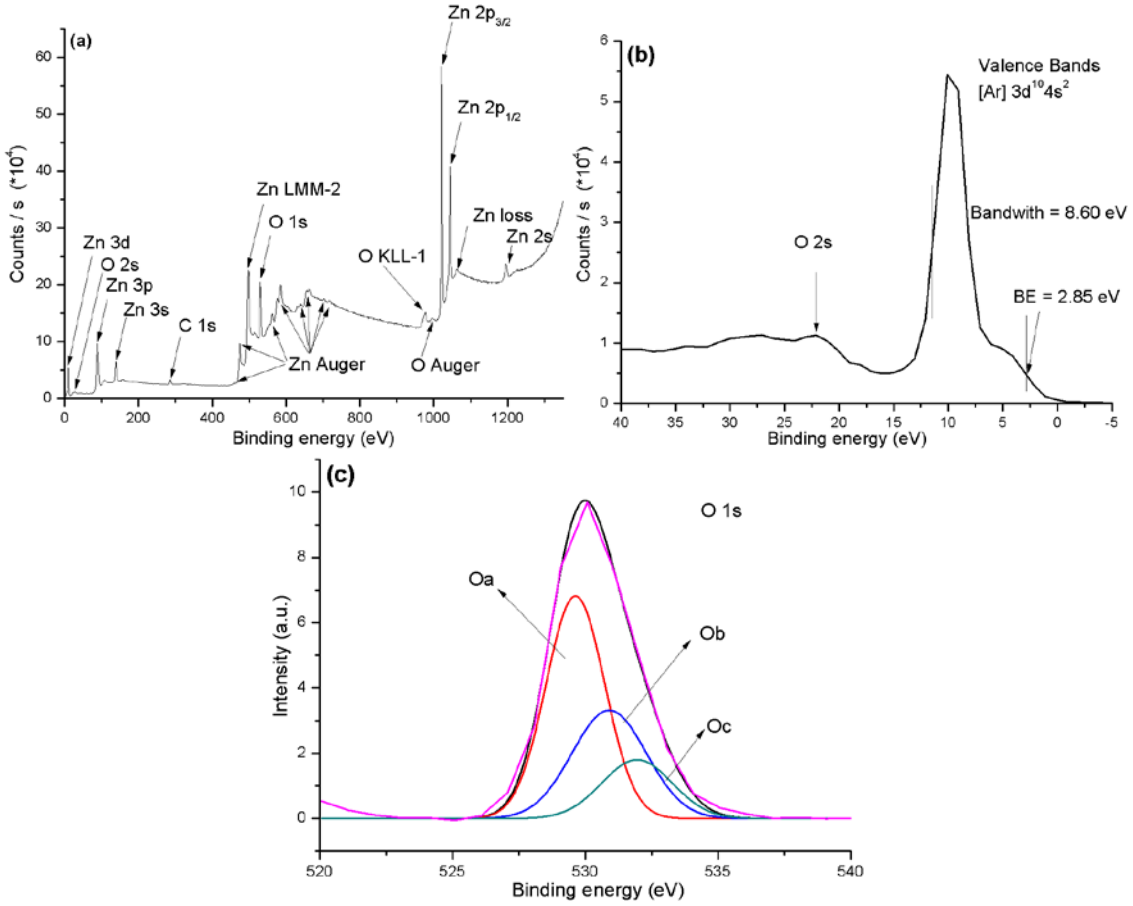


*Fig. 5 (a) The survey scan spectrum of ZnO, (b) Valence band of ZnO, (c) Oxygen 1s spectra of ZnO*

The literature is abundant in reports of ZnO photoluminescence. The photoluminescence spectra of ZnO powders usually presents two emission peaks in the UV and visible ranges [26], the relative intensity of which strongly depended on $O_2$ pressure used during the synthesis process [27].

The UV emission corresponds to the near band-edge emission (NBE) and the visible emission is commonly referred to as a deep-level or trap-state emission [28].

The relative strength of NBE to deep level defect emissions exhibits a dramatic threshold dependence on surface roughness: surface optical emission efficiency increases over tenfold as roughness decreases to unit cell dimensions, highlighting the coupled role of surface morphology and near-surface defects for high efficiency ZnO emitters [29].

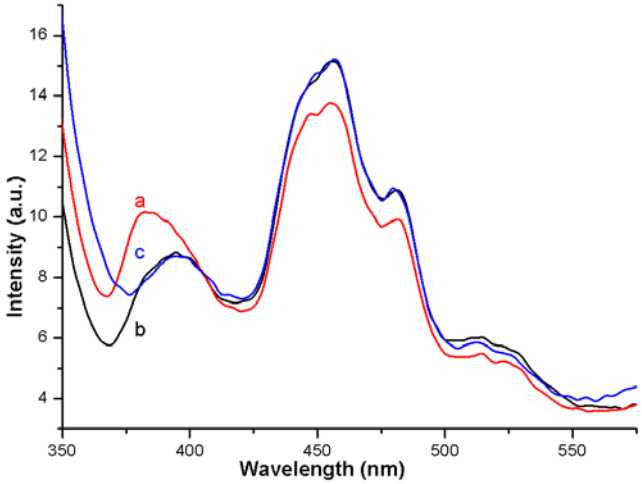


*Fig. 6. Photoluminescence spectra of ZnO nanopowder obtained for different refluxing times in methanol (12h - a, 24h - b, 36h - c) and 24h in water*

High intensity of the green and blue-green luminescence versus NBE are reported in literature whenever the luminescence spectra is recorded on powders as obtained, without further treatments (simple annealing or annealing in presence of reducing atmosphere) [30, 31].

It has been reported that the sub-band-gap emission in ZnO depends on the morphology of the nanostructures. [32-34]. A blue-green emission at 453 nm and a green emission at around 557 nm as found in literature for nest like nanoparticles [33] and emissions at 421 nm, 482 nm, and 532 nm for nanocones [34]. For as nanorods, most of the spectral weight is in the sub-bandgap, centred on 625 nm [30].

The results, figure 6, show that the as-synthesized samples have a wurtzite structure, with a weaker UV emission, and two blue-green emissions, one centred at 456 nm (with a shoulder at 446 nm) and a second at 482 nm. The weak green emission is present around 514-524 nm.

The weak UV emission at 382 nm is assigned to the free exciton emission from the wide band gap of ZnO (NBE). This peak is shifted to 392 nm upon increasing the refluxing time in methanol, indicating also the increasing size of the nanoparticles. Because the b) and c) spectra are similar, we can conclude that further refluxing time in methanol will not influence the luminescence properties of ZnO nanoparticles.

The four other emission bands at 446, 456, 482, and 524 nm in the blue-green range are defect-related emissions. The exact cause of them is still controversial. The luminescence bands at 446, 464 and 482 nm are believed to be caused by the transition from the level of the ionized oxygen vacancies to the valence band [34] or can be attributed to band-edge free excitons and bound excitons, respectively [35].

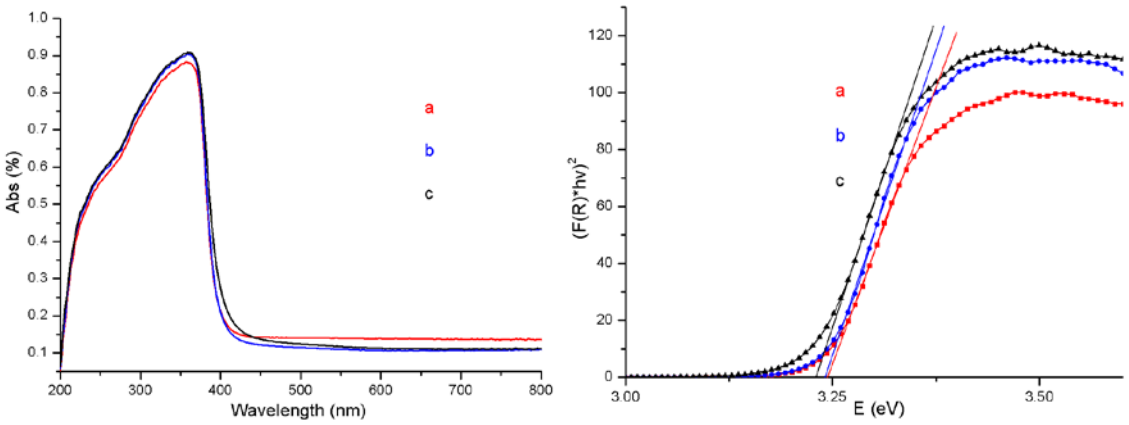


*Fig. 7. Diffuse reflectance spectra (A) and plot of the transformed Kubelka-Munk function vs. the energy (B) for the ZnO obtained by refluxing in methanol (12h - a, 24h - b, 36h - c) and 24h in water.*

The enhanced visible luminescence of the ZnO samples b) and c) can be attributed to the presence of more (OH) groups on the surface of the ZnO [36-38]. According to literatures, the enhancement of green emission is caused by the removal of electron capture centres on the surface of nanocrystals or the removal of nonradiative decay channels [39, 40].

The electronic spectra recorded for the ZnO powders obtained by refluxing 12-36h in methanol and 24h in water is presented in figure 7a.

The fundamental absorption refers to the optical transition of electrons from the valence band to conduction band and can be used to determine the nature and values of optical band gap of the nanoparticles [41, 42]. For analysis purposes the diffuse reflectance, *R*, of the sample can be related to the Kubelka-Munk function *F(R)* by the relation $F(R)=(1-R)^2/2R$, [43]. To determine the band-gap energies (Eg) for the ZnO nanoparticles, a plot of the square of the modified Kubelka-Munk function vs. the energy is presented in the figure 7b. This yields the direct band gap energy. Adopting the method proposed by Cao et al.,[44] the band-gap energies (Eg) for the ZnO nanoparticles are determined to be 3.23 - 3.24 eV, by the extrapolation to $[F(R)\cdot h\nu]^2 = 0$. The calculated band gap for ZnO is in good agreement with the literature [45, 46].

## 4. Conclusions

A synthetic method for the nanocrystalline ZnO particles in methanol solution and water without using base has been presented. The colloid process was carried out at the low temperature of 60$^o$C in methanol and 80$^o$C in water, with the solutions free from alkali ions. The ZnO particles were chemically pure in terms of cation impurities and exhibited blue-green photoluminescence by the UV excitation. TEM and XRD data sustain the formation of a single phase, monodisperse crystalline ZnO. We found that reaction time in the presence of methanol primarily influenced the size of the particles (the crystallite size varies from 10 to 40nm as estimated from the Scherrer equation), while the reaction time in the presence of water mainly influenced the ZnO purity (a 24h refluxing time being enough to yield pure ZnO nanoparticles).

**Acknowledgments**

Authors recognize financial support from the European Social Fund through POSDRU/89/1.5/S/54785 project: "Postdoctoral Program for Advanced Research in the field of nanomaterials"

## References

[1] Weißenrieder, K.S. and Muller, J. Thin Solid Films, **300**, 30-41(1997).
[2] Masai, H., Toda, T., Ueno, T., Takahashi, Y. and Fujiwara, T. Appl. Phys. Lett. **94**, 151908 (2009).
[3] Behnajady, M. A., Modirshahla, N., Ghazalian E. Digest Journal of Nanomaterials and Biostructures, **6**(1), 467 (2011).
[4] Lorenz, C., Emmerling, A., Fricke, J., Schmidt, T., Hilgendorff, M., Spanhel, L., Muller, G. J. Non-Cryst. Solids, **238**, 1(1998).
[5] Radu, A., Iftimie, S., Ghenescu, V., Besleaga, C., Antohe, V.A., Bratina, G., Ion, L., Craciun, S., Girtan, M., Antohe, S. Digest Journal of Nanomaterials and Biostructures **6**(3), 1141 (2011).
[6] Gupta, A., Bhatti, H.S., Kumar, D., Verma, N.K., Tandon, R.P. Digest Journal of Nanomaterials and Biostructures, **1**(1), 1 -9(2006).
[7] Vlad, S., Ciobanu, C., Gradinaru, R.V., Gradinaru, L.M., Nistor A. Digest Journal of Nanomaterials and Biostructures, **6**(3), 921 (2011).
[8] Mishra, P., Yadav, R.S., Pandey, A.C. Digest Journal of Nanomaterials and Biostructures **4**(1), 193 (2009).
[9] Geetha, D., Thilagavathi, T. Digest Journal of Nanomaterials and Biostructures, **5**(1), 297 (2010).
[10] Koch, U., Fojtik, A., Weller, H. and Henglein, A. Chem. Phys. Lett. **122**, 507(1985),

[11] Bahnemann, D.W., Kormann, C. and Hoffmann, M.R. J. Phys. Chem. **91**, 3789(1987),
[12] Spanhel, L. and Anderson, M.A. J. Am. Chem. Soc. **113**, 2826(1991),
[13] Honso, E., Fujihara, S., Kimura, T., Imai, H. Journal of Sol-Gel Science and Technology **29**, 71–79(2004).
[14] Golshahi, S., Rozati, S.M. Digest Journal of Nanomaterials and Biostructures **6**(1), 413 (2011).
[15] Yao, C.W., Wu, H.P., Ge, M.Y., Yang, L., Zeng, Y.W., Wang, Y.W., Jiang, Z.J. Materials Letters **61**, 3416–3420(2007).
[16] Hsieh, P.T., Chen, Y.C., Kao, K.S., Wang, C.M., Appl. Phys. A **90**, 317–321(2008)
[17] Wagner, C.D. Farad. Discuss. Chem. Soc., **60**, 291(1975)
[18] Futsuhara, M., Yoshioka, K., Takai, O. Thin Solid Films **322**, 274 (1998).
[19] Nayak, A., Banerjee, H.D. Appl Surf Sci **148**, 205–210(1999).
[20] Qian, G., Nikl, M., Bei, J., Pejchal, J., Baccaro, S., Giorgi, R., Cecilia, A., Chen, G. Opt Mater **30**, 91–94(2007)
[21] Kim, J-Y., Kim, M.R., Park, S-Y., Jang, D-J. Cryst. Eng. Comm. **12**,1803–1808(2010).
[22] Chen, M., Wang, X., Yu, Y.H., Pei, Z.L., Bai, X.D., Sun, C., Huang, R.F., Wen, L.S. Appl Surf Sci **158**, 134–140(2000).
[23] Wang, Z.G., Zu, X.T., Zhu, S., Wang, L.M. Phys. E **35**, 199(2006).
[24] Ogata, K., Koike, K., Sasa, S., Inoue, M., Yano, M. Appl Surf Sci **254**, 7708–7711(2008)
[25] Major, S., Kumar, S., Bhatnagar, M., Chopra, K.L. Appl. Phys. Lett. **49**, 394(1986)
[26] Tian, Z.R., Voigt, J.A., Liu, J., Mckenzie, B., Mcdermott, M.J., Rodriguez, M.A., Konishi, H., Xu, H.F. Nat. Mater. **2**, 821(2003).
[27] Bae, C.H., Park, S.M., Park, S.C. and Ha, J.S. Nanotechnology **17**, 381–384(2006).
[28] Huang, M.H., Wu, Y., Feick, H., Tran, N., Weber, E. and Yang, P. Adv. Mater. **13**, 113 (2001)
[29] Doutt, D., Mosbacker, H. L., Cantwell, G., Zhang, J., Song, J.J. and Brillson, L. J. Applied Physics Letters **94**, 042111(2009).
[30] Hsu, J.W.P., Tallant, D.R., Simpson, R.L., Missert, N.A. and Copeland, R.G. Applied Physics Letters **88**, 252103(2006).
[31] Yuldashev, Sh. U., Sung Woo Choi and Tae Won Kang Journal of the Korean Physical Society, **42**, S216_S218 (2003).
[32] Kwok, W. M., Djurisic, A. B., Leung, Y. H., Chan, W. K. and Phillips, D. L. Appl. Phys. Lett. **87**, 223111(2005).
[33] Li Yan, Feng Hui-yun, Zhang Nan, Liu Chuan-sheng, Trans. Nonferrous Met. Soc. China **20**, 119−122(2010).
[34] Zhang, D. H., Wang, Q. P. and Xue, Z. Y. Appl. Surf. Sci. **207**, 20 (2003)
[35] Liqianga, J., Yichuna, Q., Baiqia, W., Shudana, L., Baojianga, J., Libina, Y., Weia, F., Honggang, F. and Jiazhong, S. Sol. Energy Mater. Sol. Cells **90**, 1773 (2006).
[36] Zhou, H., Alves, H., Hofmann, D. M., Meyer, B. K., Kaczmarczyk, G., Hoffmann, A. Thomsen, C. Phys. stat. sol. (b) **229**(2), 825–828(2002).
[37] Jiang, D., Cao, L., Su, G., Qu, H., Sun, D. Applied Surface Science **253**, 9330–9335(2007).
[38] Peng, L., Wang, Y. Nanoscale Res Lett **5**, 839–845(2010).
[39] Zhang, Y., Li, Y.D. J. Phys. Chem. B **108**, 17805(2004).
[40] Liu Wentan Ren, Yong Zhang, Yin-Xi Zhang European Polymer Journal **47**, 1135–1141(2011).
[41] Rozati, S.M., Shadmani, E. Digest Journal of Nanomaterials and Biostructures **6**(2), 365-372(2011).
[42] Singh, S., Kaur, H., Pathak, D., Bedi, R.K. Digest Journal of Nanomaterials and Biostructures **6**(2), 689 – 698(2011).
[43] Kortum, G. Reflectance Spectroscopy; Springer-Verlag: New York(1969).
[44] Cao, G., Rabenberg, L. K., Nunn, C. M., Mallouk, T.E. Chem. Mater. **3**, 149–156(1991).
[45] Muthukumara, P., Selvakumarib, T.M., Ganesan, S. Digest Journal of Nanomaterials and Biostructures **5**(3), 635-639 (2010).
[46] Ezema, F.I., Nwankwo, U.O.A. Digest Journal of Nanomaterials and Biostructures **5**(4), 981 - 988(2010).